Turbulent pipe flow response to wall changes targeting specific azimuthal modes

Tyler Van Buren
Dept. of Mech. and Aerosp. Engin.
Princeton University
Princeton, NJ 08544 USA
tburen@princeton.edu

Leo H. O. Hellström
Dept. of Mech. and Aerosp. Engin.
Princeton University
Princeton, NJ 08544 USA
lhellstr@prineton.edu

Ivan Marusic
Dept. of Mech. Engin.
Melbourne University
Parkville VIC 3010, Australia
imarusic@unimelb.edu.au

Alexander J. Smits
Dept. of Mech. and Aerosp. Engin.
Princeton University
Princeton, NJ 08544 USA
asmits@princeton.edu

ABSTRACT

We present an experimental study on the response of turbulent pipe flow at $Re_\tau = 3486$ to rapid changes in pipe shape that are designed to manipulate the Large Scale and Very Large Scale Motions in wall-bounded turbulence. Stereo PIV measurements were taken 5 pipe diameters downstream of 3D printed pipe inserts designed to target specific azimuthal Fourier mode numbers $m = 3$ and 15. Direct manipulation of the flow momentum (vortex generators) and secondary flows induced by Reynolds stresses (sinusoidally varying wall shape) are considered. The designs successfully modified the mean flow to contain structures mimicking the desired Fourier mode shapes. The energy was added directly to the targeted modes, and secondary peaks in energy existed in non-targeted modes indicating nonlinear interactions. At the same time, other modes showed relatively significant losses of energy, indicating that the pipe inserts were gathering energy into predefined flow structure.

INTRODUCTION

The large-scale motions (LSMs) and the very large-scale motions (VLSMs) are the two largest know groups of organized motions in wall-bounded turbulent flows (Smits *et al.*, 2011). These motions account for a large fraction of the turbulent kinetic energy and Reynolds shear stress; and are consequently significant contributor to the turbulence production (Balakumar & Adrian, 2007). The LSMs are characterised by a low momentum region with a streamwise length up to 2-3R, where R is the pipe radius (Adrian, 2007), and are often attributed to the alignment of hairpin vortices (Adrian, 2007). The VLSMs have a typical streamwise wave length $\mathcal{O}(16R)$ but can occasionally be up to $30R$ long (Bailey & Smits, 2010; Monty *et al.*, 2007). It has been suggested that the VLSMs are a consequence of the alignment of LSMs (Kim & Adrian, 1999; Baltzer *et al.*, 2013; Hellström *et al.*, 2015), where the underlying alignment mechanism may be due to linear and non-linear processes (del Álamo & Jiménez, 2006).

Bailey & Smits (2010) showed that the spanwise behaviour of the VLSMs and LSMs in a pipe flow are similar, where the dominant feature extends over one-third of the circumference in the azimuthal direction and one radius in the radial direction. They further showed that this single structure contributed to both the VLSM and LSM wave lengths.

Hellström *et al.* (2011), Hellström & Smits (2014), and Hellström *et al.* (2015) showed that proper orthogonal decomposition (POD) can be used to examine the characteristics of large-scale energetic motions and their streamwise evolution. In pipe flow, the azimuthal direction can be decomposed into Fourier modes (m), while the, non-homogeneous radial direction is decomposed using POD and ranked by its energy. Hellström & Smits (2014) supported the findings by Bailey & Smits (2010) and showed that the third azimuthal Fourier mode ($m = 3$), characterized by three pairs of low and high momentum azimuthal structures, contained the most turbulent kinetic energy (similarly shown in Baltzer *et al.* (2013)).

Hellström *et al.* (2016) expanded on this work and found that the wall-normal height of a radial POD mode scaled with its azimuthal wave length, where these structures were found to be self-similar for $m \in [5,\ 32]$ for $Re_\tau = 2460$. The lower bounds of this range stemmed from the geometric limitations of the pipe (Chung *et al.*, 2015) and the structures at the upper bound were influenced by viscosity and not expected to be self-similar.

Given that the broad features of the energetic motions in pipe flow are described a relatively small number of modes, the question arises whether this knowledge can be used to formulate a control strategy. Here, we explore how the structures in a turbulent pipe flow respond to a modification of the pipe geometry where the modification is designed to target the energetic modes described in Hellström & Smits (2014). By altering the shape of the pipe cross-section, we attempt to excite single or multiple modes at a time and measure the flow response. We use two strategies: (1) direct addition of streamwise vorticity via vortex generators; and (2) creating spanwise gradients of the Reynolds stress to introduce mean vortical structure through Prandtl's secondary flow of the second kind (Prandtl, 1952; Perkins, 1970; Anderson *et al.*, 2015).

We will show that the mean flow can be changed to produce structures similar to the energetic motions in turbulent pipe flow, and that energy can be added at specific azimuthal wavelengths. We also observe changes in the energy of the non-targeted modes, which implies the presence of non-linear interactions between these wavelengths.

EXPERIMENTAL SETUP

Experiments were conducted in a pipe with an inner diameter of $D = 38.1$ mm and a development length of $220D$. The bulk velocity was fixed at $U_b = 4.18$ m/s corresponding to a Reynolds number $Re_D = U_b D/\nu = 158\,600$ and a friction Reynolds number of $Re_\tau = u_\tau R/\nu = 3486$ where u_τ is the friction velocity and ν is the kinematic viscosity. The working fluid was water. An access port was installed immediately upstream of the test section, in which 3D

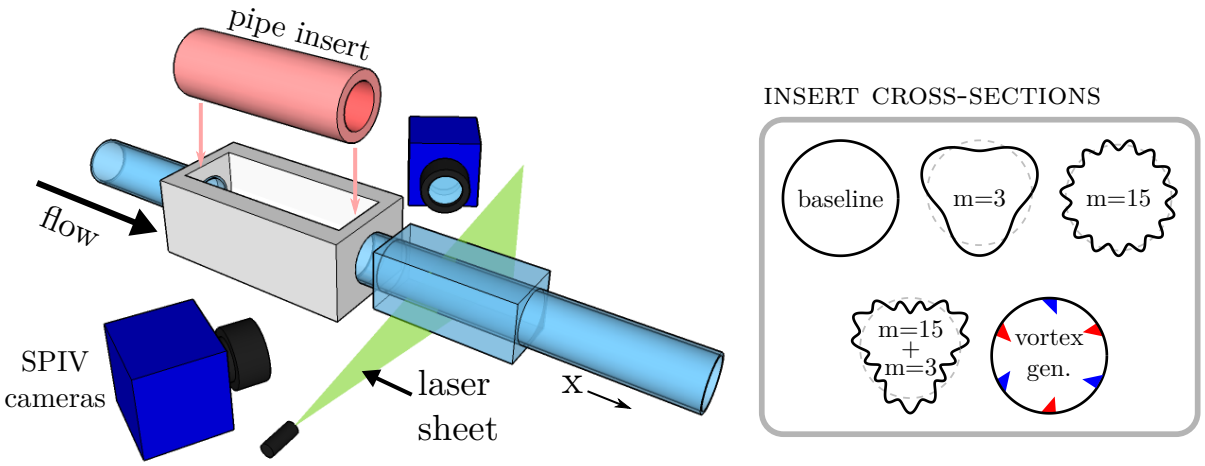

Figure 1. Left: schematic of the experimental setup. Right: pipe insert center cross-sections; Cases 1 (baseline) to 5 (vortex generators).

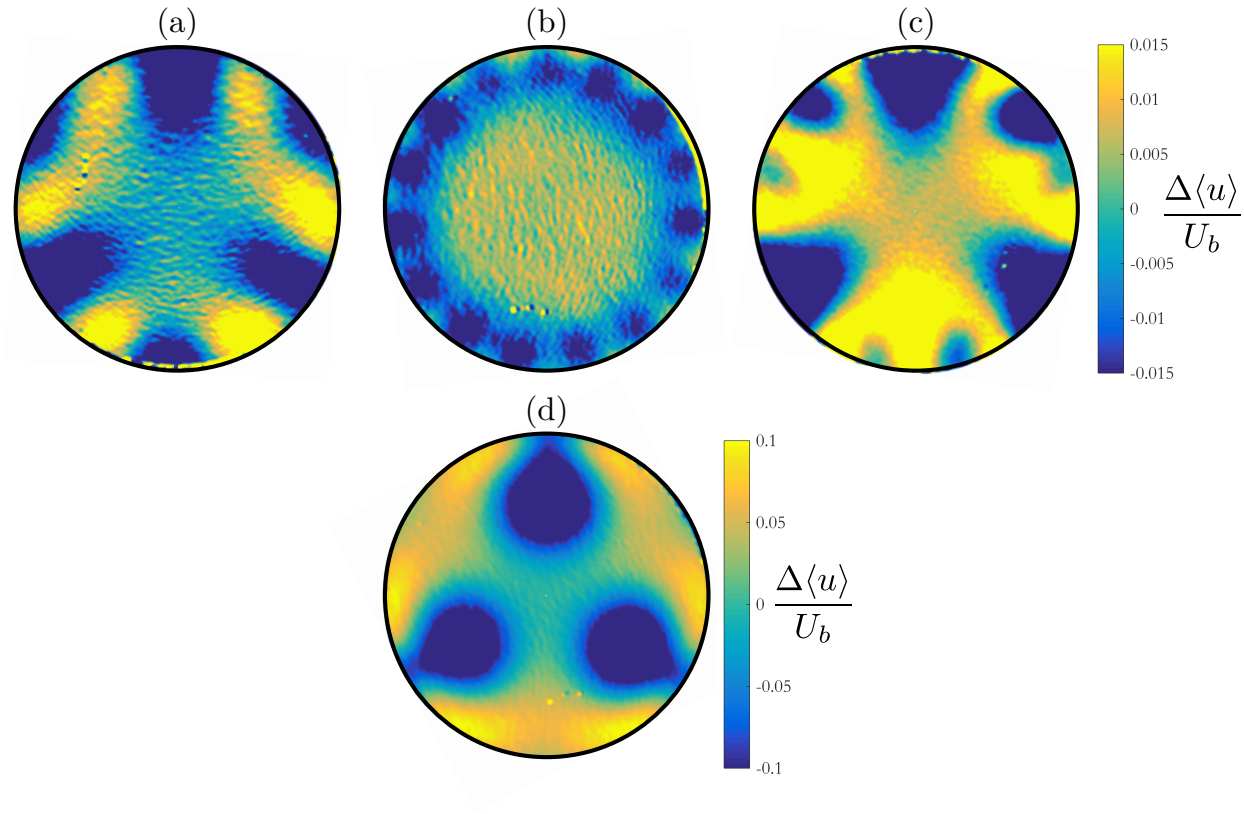

Figure 2. Change in the time-averaged local streamwise velocity with respect to the baseline (Case 1). (a) Case 2, $m = 3$; (b) Case 3, $m = 15$; (c) Case 4, $m = 3$ superimposed with $m = 15$; (d) Case 5, vortex generators.

printed PLA pipe segments of length $l = 8R$ could be inserted. The experimental setup is shown in figure 1.

Five different inserts were used: Case I, a baseline insert with a simple circular cross-section); Cases 2, 3, and 4 where gradual changes in geometry were used to generate streamwise secondary motions by Reynolds stress gradients; and Case 5 that used six evenly distributed triangular-type vortex generators each of height $0.2R$, length $0.5R$, where the angle made by each vortex generator with the incoming flow direction flipped between $+15^\circ$ and -15° to create three counter-rotating vortex pairs.

The wall geometry for Cases 2 to 4 was governed by an azimuthal Fourier mode (m), where the perturbation amplitude grows as a cosine wave with its streamwise location. The wall location is more generally defined as:

$$r(\theta, m, x) = R + \frac{\cos(2\pi \frac{x}{8R}) + 1}{2} \sum_m a_m \sin(m\theta), \qquad (1)$$

where a_m is the perturbation amplitude, $\theta \in [0,\ 2\pi)$ and $x \in [-4R,\ 4R]$. For Case 2 $m = 3$, $a_3 = 0.2$; for Case 3 $m = 15$, $a_{15} = 0.1$, and Case 4 used the superposition of $m \in \{3,\ 15\}$. For these perturbation amplitudes, the average angle of the wall displacement with streamwise position is 2.8° and 1.4° for the a_3 and

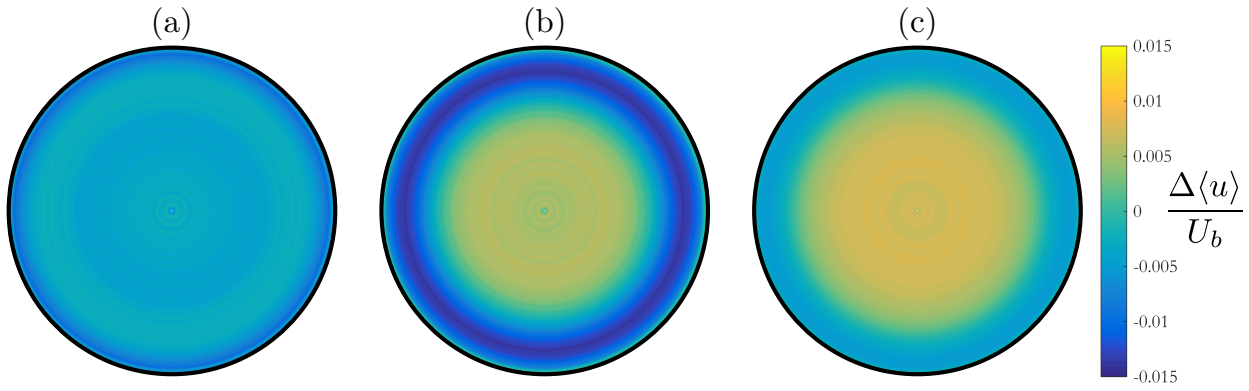

Figure 3. Azimuthal average of the streamwise velocity with the baseline local time-averaged velocity subtracted. (a) Case 2, $m = 3$; (b) Case 3, $m = 15$; (c) Case 4, $m = 3$ superimposed with $m = 15$.

a_{15} cases, respectively, and were considered to be smooth changes. For these cases, the maximum change in cross section area can be expressed as $\Delta A = \frac{1}{2}\sum_m (\frac{a_m}{R})^2$, and is at most 2.5%.

The flow measurements were taken using stereoscopic particle image velocimetry at a position $227D$ downstream of the pipe entrance and $5D$ from the pipe insert center. Images were taken using two 5.5 mega-pixel sCMOS cameras with a dual-pulsed 50 mJ Nd:YAG laser to illuminate the flow seeded with 10 μm hollow glass spheres. To minimize image distortion, the pipe was surrounded by a water-filled acrylic box at the measurement location. Four sets of 2000 images were acquired at 25 Hz for each test case and processed using a multi-pass cross-correlation method with a final interrogation window size of 16×16 pixels with 50% overlap. The final vector grid spacing was 0.14 mm.

RESULTS

We begin by exploring the change in the mean streamwise velocity with respect to the baseline, $\Delta\langle u\rangle$, for each pipe insert shown in figure 2, where u represents the streamwise velocity component. The vortex generators (Case 5) exhibit the strongest change in the mean streamwise velocity ($\leq 10\%$), with three distinct regions of flow deficit induced by the three pairs of vortices. The impact of the Reynolds stress inducers (Cases 2 to 4) on the flow is less ($2-5\%$), but the intended flow structures are still evident. Cases 2 and 3, designed induce structures similar to $m = 3$ and $m = 15$, do produce 3 and 15 regions of velocity deficit, respectively. We also see the presence of these azimuthal structures for the case of the superimposed modes, where $m \in \{3,\ 15\}$ (Case 4).

Figure 3 shows the azimuthal average of the baseline subtracted velocity for the same cases. Cases 3 and 4 that target $m = 15$ generate near-wall regions of velocity deficit with a velocity increase in the wake region. This is why the lower velocity regions appear to be more dominant in the near-wall region than the higher velocity regions in figure 2.

Decomposing the flow by a Fourier series in the azimuthal direction allows us to sort the flow energy based upon azimuthal wavenumber, m. Here we use the power spectral density (PSD) $\phi_{uu} = \langle \hat{u}(m,r,t)\cdot\hat{u}^*(m,r,t)\rangle_t$ normalized by the friction velocity u_τ^2, premultiplied with the azimuthal mode number m, where $*$ represents the complex conjugate. Figure 4 shows the premultiplied PSD for the baseline, smooth wall case. High energy is concentrated near lower mode numbers, with a peak at $y/R = 0.2$ and $m = 5$.

Interestingly, this peak mode number corresponds to the lower bound of the structure self-similarity range shown in Hellström *et al.* (2016) for $Re_\tau = 2460$, while the upper bound of the mode number range corresponds to where the structure sizes approach that

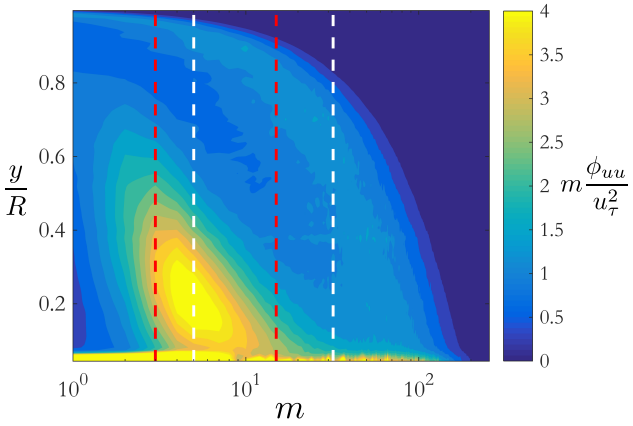

Figure 4. Premultiplied power spectral density for the baseline (smooth pipe, Case 1). Red dashed lines show the locations of targeted modes ($m = 3, 15$) and white dashed lines show the limits of self-similarity from Hellström *et al.* (2016) for $Re_\tau = 2460$ ($m \in \{5,\ 32\}$).

of the near-wall viscous dissipation region. These limits are marked with broken white lines in figure 4. Evidence for the self-similarity can be seen here in how the contour variations are logarithmically approaching the wall (which appear as an exponential approach in the semi-log plot in figure 4). The leading edge of the high energy region agrees well with Hellström & Smits (2014), where $m = 3$ was found to have the largest portion of turbulent kinetic energy, indicated with the left broken red line in figure 4. The right broken red line indicates $m = 15$, which is in the middle of the self-similar region and chosen with $m = 3$ to be the mode numbers targeted by the particular perturbations used here.

Now we consider the change in PSD with respect to the baseline, $\Delta\phi_{uu}$, for the case with the vortex generators (Case 5). Figure 5 shows that there is a very large, distinct peak at $m = 3$, which is the intended mode of excitation. Other, smaller peaks occur at $m \in \{6,\ 9,\ 12\}$, which decay in magnitude and approach the wall with increasing mode number. These secondary peaks are the harmonics of the excited mode $m = 3$, and exist due to the non-linear interactions between mode numbers where $m_1 = m_2 \pm m_3$. For example, the peak at $m = 6$ is a consequence of the interaction between structures with $m = 3$ and the interaction between $m \in \{3,\ 9\}$, and so on. Similarly, the peak at $m = 9$ is generated by, for instance, the

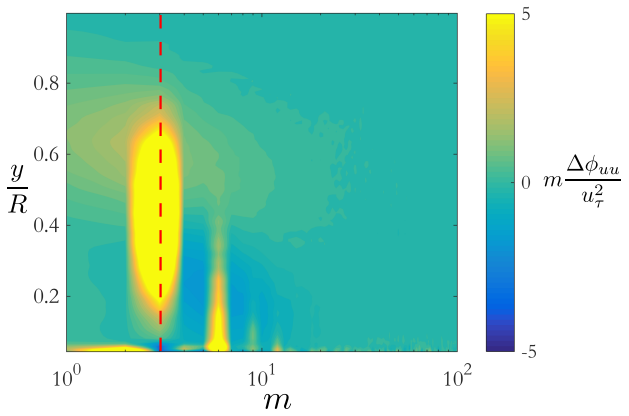

Figure 5. Change in premultiplied power spectral density relative to the baseline for the vortex generator case targeting $m = 3$ (Case 5). Red dashed line shows $m = 3$.

interaction between $m = \in \{3\ ,6\}$. These types of non-linear interactions have also recently been studied in turbulent boundary layers (Duvvuri & McKeon, 2016).

More subtly, there is a suppression of energy with respect to the baseline in the mode numbers between the peaks, indicating that the excitation of $m = 3$ has removed energy from other structures that would normally occur.

Figure 6 shows the change PSD relative to the baseline for the cases that induce Reynolds stresses to target modes $m = 3$ and 15 (Cases 2 to 4). Generally, the changes are much weaker than the case with the vortex generators (note the change in color axis limits), which are consistent with the mean flow changes shown in figure 2. For the cases individually targeting modes $m = 3$ and 15 (figures 6a-b), there are distinct peaks of energy near those mode numbers. Much like the vortex generator case, there is a secondary peak at $m = 6$ for the case targeting $m = 3$. For the case targeting $m = 15$, the energy peak is slightly shifted to a lower mode number $m = 12$. This could be a result of the interaction with the most prominent of the naturally occurring organized motions, $m = 3$.

There is also a relatively significant decrease in turbulence kinetic energy in the non-targeted modes, similar in magnitude to the energy added to the targeted modes. For the case targeting $m = 15$ (figure 6b), all of the lower mode numbers have reduced energy. This mechanism opens up the possibility of suppressing a range of turbulent structures by targeting one predefined mode number. It should also be noted that these structures remain present for far longer than their own length scales. The wall-normal length scale for $m = 15$ is $\mathcal{O}(0.3R)$, while the current data set is acquired $10R$ downstream the peak magnitude of the perturbation, which corresponds to $\mathcal{O}(30)$ structure heights.

Figure 6c is the case which simultaneously targets $m = 3$ and 15. Similarly to the $m = 15$ case in figure 6b, there is a region of relatively low turbulence kinetic energy for $m < 12$. This region seemingly suppresses the main peak at $m = 3$ and the secondary peak at $m = 6$, which are much less evident here than in the individual $m = 3$ case. There is still a strong peak at $m = 12$, which is likely the interaction of the targeted peaks at $m = 3$ and $m = 15$.

The energy distribution can be thought of as the superposition of energy from the separate cases together with their non-linear interactions. These non-linear interactions are highlighted in figure 7, which presents the leftover PSD if the cases independently targeting modes $m = 3$ and 15 (figures 6a-b) are subtracted from the case simultaneously targeting both (figure 6c). We see that there is

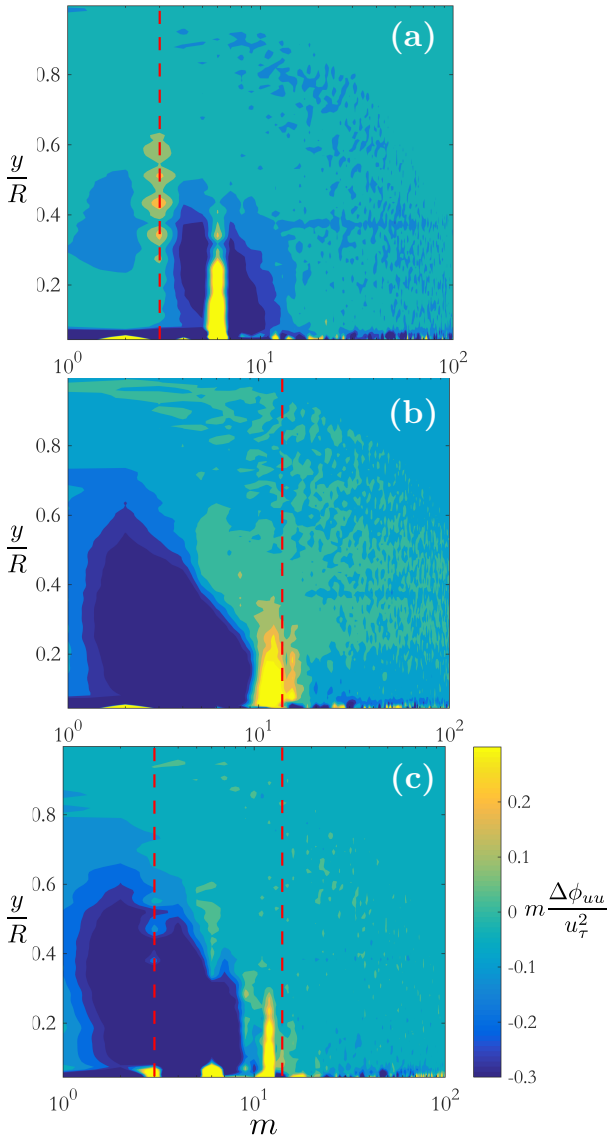

Figure 6. Change in premultiplied power spectral density relative to the baseline for (a) Case 2, $m = 3$; (b) Case 3, $m = 15$; (c) Case 4, $m = 3$ superimposed with $m = 15$. Red dashed lines show $m = 3$ and 15.

reduced energy in modes $m = 6$ and 12, but an increase in energy for the adjacent modes.

CONCLUSIONS

We have experimentally explored the flow's response to a change in cross-sectional shape designed to target specific modes using two strategies: a direct addition of momentum deficit through vortex generators, and secondary flow induction through Reynolds stresses.

The vortex generators substantially changed the mean flow, producing three distinct regions of momentum deficit equally spaced azimuthally. This resulted in a sharp increase in the energy at Fourier mode $m = 3$ and secondary energy peaks at $m \in \{3,\ 6,\ 9,\ 12\}$, where the energy and size decreased with increasing mode numbers.

The Reynolds stress inducers (Cases 2 to 4) had a smaller impact on the mean flow, but still created structures that corresponded to the modes that were specifically targeted, $m = 3$ and 15. Each

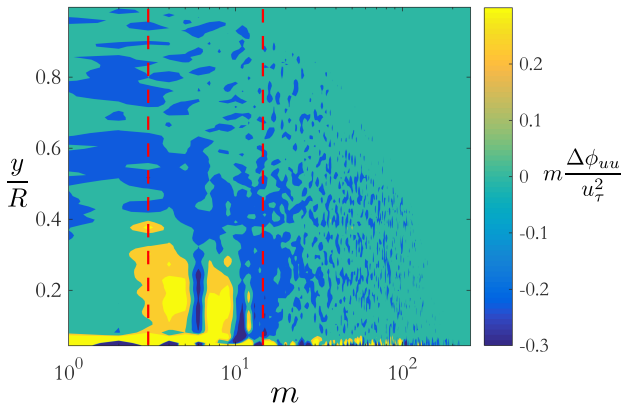

Figure 7. Change in premultiplied power spectral density for Case 4 targeting Fourier modes $m \in \{3,\ 15\}$ with the individual cases targeting $m = 3$ (Case 2) and 15 (Case 3) subtracted. Red dashed lines show $m = 3$ and 15.

case produced corresponding increases in energy at the targeted modes, while also often reducing energy in the surrounding modes. Therefore a mechanism has been identified to suppress a range of turbulent structures by targeting one predefined mode number. In addition, by simultaneously targeting $m = 3$ and 15 we found nonlinear interactions between the two induced modes, where the resulting structures contain similar energy levels to the directly induced modes.

Future work will include further analysis of the interaction between targeted and non-targeted modes, downstream development of the induced structures.

ACKNOWLEDGMENTS

This work was supported by the Office of Naval Research grant number N00014-15-1-2402 (Program Director Tom Fu and Program Manager Ron Joslin), as well as the Australian Research Council.

REFERENCES

Adrian, R. J. 2007 Hairpin vortex organization in wall turbulence. *Physics of Fluids* **19** (4), 041301.

del Álamo, J. C. & Jiménez, J. 2006 Linear energy amplification in turbulent channels. *Journal of Fluid Mechanics* **559**, 205–213.

Anderson, W., Barros, J. M., Christensen, K. T. & Awasthi, A. 2015 Numerical and experimental study of mechanisms responsible for turbulent secondary flows in boundary layer flows over spanwise heterogeneous roughness. *Journal of Fluid Mechanics* **768**, 316–347.

Bailey, S. C. C. & Smits, A. J. 2010 Experimental investigation of the structure of large- and very large-scale motions in turbulent pipe flow. *Journal of Fluid Mechanics* **651**, 339–356.

Balakumar, B. J. & Adrian, R. J. 2007 Large- and very-large-scale motions in channel and boundary-layer flows. *Philosophical Transactions of the Royal Society of London. Series A, Mathematical, Physical and Engineering Sciences* **365**, 665–681.

Baltzer, J. R., Adrian, R. J. & Wu, X. 2013 Structural organization of large and very large scales in turbulent pipe flow simulation. *Journal of Fluid Mechanics* **720**, 236–279.

Chung, D., Marusic, I., Monty, J. P., Vallikivi, M. & Smits, A. J. 2015 On the universality of inertial energy in the log layer of turbulent boundary layer and pipe flows. *Experiments in Fluids* **56** (7), 1–10.

Duvvuri, S. & McKeon, B. J. 2016 Nonlinear interactions isolated through scale synthesis in experimental wall turbulence. *Physical Review Fluids* **1** (3), 032401.

Hellström, L. H. O., Ganapathisubramani, B. & Smits, A. J. 2015 The evolution of large-scale motions in turbulent pipe flow. *Journal of Fluid Mechanics* **779**, 701–715.

Hellström, L. H. O., Marusic, I. & Smits, A. J. 2016 Self-similarity of the large-scale motions in turbulent pipe flow. *Journal of Fluid Mechanics* **792**, R1.

Hellström, L. H. O., Sinha, A. & Smits, A. J. 2011 Visualizing the very-large-scale motions in turbulent pipe flow. *Physics of Fluids* **23** (1), 011703.

Hellström, L. H. O. & Smits, A. J. 2014 The energetic motions in turbulent pipe flow. *Physics of Fluids* **26** (12), 125102.

Kim, K. C. & Adrian, R. J. 1999 Very large-scale motion in the outer layer. *Physics of Fluids* **11** (2), 417–422.

Monty, J. P., Stewart, J. A., Williams, R. C. & Chong, M. S. 2007 Large-scale features in turbulent pipe and channel flows. *Journal of Fluid Mechanics* **589**, 147–156.

Perkins, H. J. 1970 The formation of streamwise vorticity in turbulent flow. *Journal of Fluid Mechanics* **44** (04), 721–740.

Prandtl, L. 1952 *Essentials of Fluid Dynamics*. Hafner Pub. Co.

Smits, A. J., McKeon, B. J. & Marusic, I. 2011 High-Reynolds number wall turbulence. *Annual Review of Fluid Mechanics* **43**, 353–375.